Brillouin light scattering study of ferromagnetically coupled Cu/Fe(110)/Cu/Fe(110)/Cu/Si(111) heterostructures: Bilinear exchange magnetic coupling

G. Gubbiotti and G. Carlotti
Istituto Nazionale per la Fisica della Materia, Dipartimento di Fisica dell'Università, Via Pascoli, I-06100 Perugia, Italy

A. Montecchiari and M. De Crescenzi
Istituto Nazionale per la Fisica della Materia, Dipartimento di Matematica e Fisica dell'Università, Via Madonna delle Carceri, I-62032 Camerino, Italy

R. Zivieri, L. Giovannini, and F. Nizzoli
Istituto Nazionale per la Fisica della Materia, Dipartimento di Fisica dell'Università, Via Paradiso 12, I-44100 Ferrara, Italy
(Received 8 May 2000; revised manuscript received 2 August 2000)

Epitaxial Cu(60 Å)/Fe(20 Å)/Cu(d_{Cu})/Fe(60 Å)/Cu(60 Å) heterostructures with the Cu spacer thickness d_{Cu} ranging between 0 and 33 Å have been grown on 7×7 reconstructed surface of Si(111) substrates. Fcc(111) Fe films grow epitaxially on the Cu(111) buffer layer up to a thickness of 6–8 Å, while, for larger thicknesses, one observes the appearance of three-dimensional bcc Fe(110) domains in the Kurdjumov-Sachs orientation. Brillouin light scattering (BLS) from thermally excited spin waves has been exploited in order to study the interlayer exchange coupling between the two Fe films at room temperature. The experimental spin-wave frequency dependence on the applied magnetic field is simulated using a simple model which includes first-order intrinsic volume and interface anisotropies and takes the bilinear exchange interaction between the two ferromagnetic layers into account. We have found that for thicknesses of the Cu spacer larger than 6 Å, the Brillouin spectrum consists of two spin-wave modes due to the Fe double layered structure which depends on the Cu-layer thickness. The coupling is found to be ferromagnetic for the whole range of Cu spacer thicknesses investigated. Using the magnetic parameters determined by the above analysis, we have carried out a detailed calculation of the BLS cross section assuming the dynamic magnetization to be constant across each magnetic film. A very good agreement between the calculated and the measured cross sections has been obtained.

I. INTRODUCTION

In the last decade different experimental techniques have been applied to the investigation of exchange coupling in ferromagnetic bilayer samples. In particular, the earliest Brillouin light scattering investigations of interlayer coupling in polycrystalline Fe/Cu/Fe bilayers were performed by Grünberg *et al.*[1–3] More recently, Brillouin light scattering experiments on exchange coupled ultrathin Fe films separated by epitaxial Cu(001) grown on Ag(001) single crystal have been performed by Cochran *et al.*[4] They found that the interlayer exchange coupling changes from ferromagnetic to antiferromagnetic as the Cu layer thickness was increased above nine monolayers. Subsequently, Heinrich *et al.*[5] studied the interlayer exchange by ferromagnetic-resonance (FMR) and surface magneto-optical Kerr effect (SMOKE) in bcc Fe/Cu/Fe(001) structures grown on Ag(001), Cr(001), and Fe(001) substrates. They found that the exchange coupling exhibits a short-wavelength oscillatory behavior from a ferromagnetic to an antiferromagnetic (AF) interaction. To this respect, we notice that most reports on oscillatory magnetic coupling through nonmetal spacers have concerned the (100) orientation, whereas coupling through the (111) orientation has been somewhat more difficult to observe. In their Mössbauer study on the magnetic coupling on Fe(110)/Cu(111) multilayers, Freeland *et al.*[6] measured a ferromagnetic interlayer exchange coupling over the whole investigated range of thicknesses of the Cu spacer. Brillouin intensities calculations in Fe/Au/Fe coupled films[7] based upon an extension of the approach applied to a single film[8] have shown the effect of the interlayer coupling constant on the scattered light intensities. Brillouin cross-section calculations based on a partial wave approach[8] with variable dynamic magnetization across ferromagnetic films have been performed by Roussigné and co-workers[9] on Co/Cu/Co and Co/Au/Co structures to obtain magnetic anisotropy and interlayer exchange coupling. An oscillatory behavior of the interlayer exchange as a function of Cu thickness has been found.

In previous papers, we have shown that epitaxial Cu/Fe/Cu heterostructures with Fe thickness between 2.5 and 110 Å can be successfully grown on the 7×7 reconstructed surface of Si(111), using the metal-metal epitaxy on silicon technique (MMES).[10,11] The growth of ferromagnetic films on semiconductors offers the opportunity for many new technological applications in the field of sensors and spin electronics.[12] Fcc(111) Fe films grow epitaxially on a Cu(111) buffer layer, deposited on the 7×7 reconstructed surface of Si(111), up to a thickness of 6–8 Å. For larger thicknesses one observes the appearance of three-dimensional bcc Fe(110) domains in the Kurdjumov-Sachs (KS) orientation characterized by a high magnetic moment. The KS orientation is a special case of the one-dimensional matching between bcc(110) and fcc(111) with sides of the rhombic unit meshes of the film parallel to those of the

substrate.[13,14] The growth of bcc(110) Fe domains in KS orientation yields the appearance of new satellite spots in the low-energy electron diffraction (LEED) pattern superimposed to the hexagonal net of pseudomorphic Fe on Cu(111).[15,16] Low-temperature (20–150 K) Kerr effect measurements revealed that Fe films thinner than 5–6 Å are ferromagnetic with an easy axis magnetization perpendicular to the film plane. With increasing Fe thickness, in coincidence with the fcc-to-bcc structural transformation, the easy axis switches to the in-plane orientation over a finite range of thickness.[17]

In this paper, we extend the study to the case of two iron films separated by a stepped layer of Cu with thicknesses d_{Cu} ranging between 0 and 33 Å in steps of 3 Å. In the case of $d_{\mathrm{Cu}}=0$ the system consists of a single iron film 80 Å thick. In order to interpret the Brillouin light scattering (BLS) data and to study the interlayer exchange coupling, we have extended the constant dynamic magnetization model applied to a single film to a double film. The generalization has been performed including in the Hamiltonian the bilinear coupling. This permitted us to achieve a very satisfactory reproduction not only of the measured spin wave frequencies, but also of the experimental Brillouin cross section.

The paper is organized as follows. Section II describes the Brillouin experimental setup. Section III illustrates the sample preparation. Section IV presents the theoretical model used to reproduce the experimental data. Section V compares the calculations with the experimental results, while conclusions are outlined in the last Sec. VI.

II. BRILLOUIN EXPERIMENT

For the BLS experiment a Sandercock-type (3+3)-pass tandem Fabry-Perot interferometer characterized by a finesse of about 100 and a contrast ratio[18] higher than 5×10^{10} is used to separate the inelastically scattered light from the elastic scattered light. *P*-polarized light, with power ranging between 100 and 200 mW, from a 5145-Å Ar^{+}-ion laser is focused onto the sample surface and the scattered light detected with typical sampling time of about 0.5 h. A sketch of the experimental apparatus can be found in Ref. 19. BLS spectra were recorded in the backscattering configuration using the same objective to focalize light onto the sample surface and to collect back light to the interferometer. The conservation of momentum in the photon-magnon interaction implies that the spin-wave wave vector parallel to the film surface is linked to the optical wave vector k_{i} and to the angle of incidence θ_{i} by the equation: $q=2k_{\mathrm{i}}\sin\theta_{\mathrm{i}}$. All spectra were recorded in air at room temperature at an incidence angle of light $\theta_{\mathrm{i}}=45°$ and therefore $q=1.73\times10^{5}$ cm^{-1}. The sample was placed between the poles of an electromagnet used to produce a dc magnetic field H with maximum intensity of 6.0 kOe. This field was parallel to the film surface and perpendicular to the plane of incidence of light.

III. SAMPLE PREPARATION AND STRUCTURAL CHARACTERIZATION

Cu(60 Å)/Fe(20 Å)/Cu(d_{Cu})/Fe(60 Å)/Cu(60 Å)/Si(111) films, with d_{Cu} interlayer film thickness ranging between 0 and 33 Å, were prepared in a ultrahigh vacuum (UHV) system with a base pressure of 5×10^{-11} Torr, equipped with standard preparation and characterization facilities such as low-energy electron diffraction (LEED), Kikuchi electron diffraction (KED) and Auger electron spectroscopy (AES). The surface of the Si(111) crystal (p type, 0.1 Ω cm, $1\times1\times0.02$ cm^3) has been cleaned following the procedure described in Ref. 20. To obtain the best conditions of epitaxial growth and to avoid the formation of Fe silicides and/or metallic islands, a Cu buffer layer 60 Å thick was deposited at room temperature on the clean Si substrate before the evaporation of the 60-Å-thick Fe film.[10,21] On top of the 60-Å-thick Fe film, we have deposited a stepped Cu interlayer with step thickness of 3 Å and lateral width of 3 mm instead of an uniform Cu film. This procedure reduces the preparation time and the scattering of data resulting from variations of the deposition conditions. The growth of a stepped layer was achieved placing a retractable shutter between the sample holder and the evaporation cells. As a result, an increasing area of the sample is exposed to the flux from Cu source and covered by the deposition materials. On top of the Cu interlayer, a second Fe film, 20 Å thick, was evaporated and finally a Cu protective capping layer 60 Å thick was deposited on top of the second Fe film, in order to prevent it from oxygen contamination during *ex situ* measurements. The evaporation of metallic layers onto the Si substrate, kept at room temperature, was obtained heating the source material above its melting point by flowing a current of several amperes in filaments (purity 99.999 %) of 1 mm diameter. The pressure during deposition rose to a few 10^{-10} Torr. The growth rate, for both Cu and Fe, was about 0.1 Å/s. For each of the materials the thickness was measured by a calibrated quartz microbalance. Auger spectra have been carried out to check the cleanliness of the substrate and the atomic purity of the deposited overlayers. Sizable interdiffusion between metals and silicon or formation of metallic islands can be excluded because only the characteristic Auger features of the deposited materials have been observed.

Concerning the structural characterization, we show in Fig. 1 the LEED patterns of the two iron films, taken at the same energy (64 eV) for a Cu interlayer thickness of 18 Å. The LEED patterns produced by the growth of Fe bcc(110) domains in KS orientation on Fe fcc(111) films are expected to consist of a cluster of satellite spots placed in a position corresponding to the hexagonal net of the underlying Fe layers pseudomorphic with Cu(111).[11] Since the spot intensities vary with electron energy, not all the five spots are clearly observable at the same energy. In our case, because of the large Fe film thickness with respect to the critical thickness (6–8 Å) where the bcc(110) domains start to appear, the cluster of spots appear to be broadened. The LEED pattern of the Cu interlayer is sixfold symmetric as that of the Cu buffer layer and is rotated by 30° with respect to the that of Si(111).[10,21] The reason of the sixfold symmetry of the Cu buffer layer when deposited on the 7×7 reconstructed surface of Si(111), instead of the threefold expected one of a Cu(111), are discussed in great details in Ref. 11. On the basis of the chemical and structural results, we are particularly confident of the continuity of the film, well-defined crystal orientation and absence of an interdiffusion process in our heterostructures.

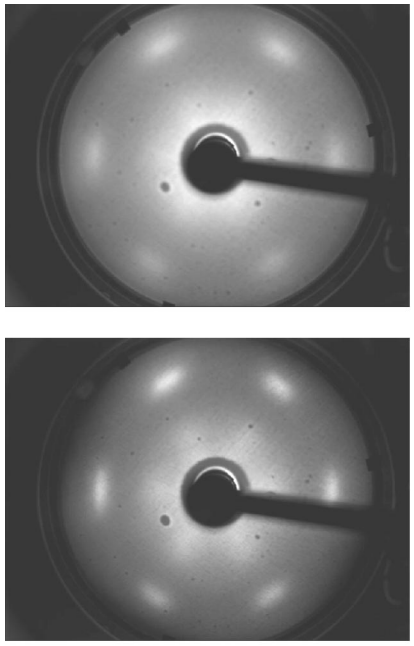

FIG. 1. LEED patterns of Cu/Fe/Cu/Fe/Cu/Si(111) heterostructures of the two Fe films, (a) 60 and (b) 20 Å thick, in the case of interlayer Cu thickness of 18 Å.

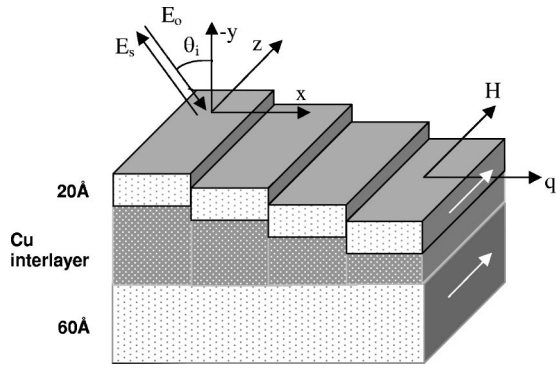

FIG. 2. The sample geometry pictorially represented together with the backscattering configuration; the directions of both the incident $\mathbf{E}_0$ and the scattered, $\mathbf{E}_s$ electric fields are depicted. $\theta_i = 45°$. Film *A*: Fe (110) = 20 Å; Cu stepped interlayer; film *B*: Fe (110) = 60 Å. The external field *H* and the parallel propagation magnon wave vector *q* are shown. The white arrows in each ferromagnetic film indicate the direction of the static magnetizations, respectively, $\mathbf{M_A}$ and $\mathbf{M_B}$, at all applied fields. The Cu interlayer thickness varies from 0 to 33 Å. Steplike variations are of 3 Å.

IV. THEORETICAL MODEL

In the limit of thin films and, in particular, for iron films with thickness below 100 Å, it is a valid approximation to suppose the dynamic magnetization constant across each layer.[22] As depicted in Fig. 2, the static magnetizations of layers *A* and *B*, respectively $\mathbf{M}_A$ and $\mathbf{M}_B$, lie in the films plane and are parallel to the applied magnetic field $\mathbf{H}$. Due to the isotropic nature of the sample in the direction parallel to the film plane, the anisotropy energy assumes a phenomenological form which depends only on the polar angle θ and is not a function of the azimuthal angle ϕ.[23,24] Therefore the density energy of the lth layer is given by

$$U_l = -K_l^{\mathrm{eff}(1)}\cos^2\theta - \mathbf{H}\cdot\mathbf{M}_l, \quad l = A,B, \tag{1}$$

where the first term on the right side is the anisotropy energy U_l^{an} with $K_l^{\mathrm{eff}(1)} = K_l^{\mathrm{V}} + 2K_l^{\mathrm{s}}/d_l - 2\pi M_l^2$ the first-order anisotropy constant. K_l^{V} and K_l^{s} are the volume and the interface anisotropy constants, respectively, and d_l is the film thickness, whereas $-2\pi M_l^2$ refers to the shape anisotropy of the lth film which is responsible for the in-plane magnetization. We have not taken into account the second-order anisotropy contribution, because it turned out to be negligible with respect to the first-order one, as observed in single iron film.[11] The magnetic anisotropy field is so modeled by first-order anisotropy energy contribution, only.

The total energy per unit area of the ferromagnetically coupled bilayer system may be expressed as

$$E = d_A U_A + d_B U_B - J_1 \frac{\mathbf{M}_A\cdot\mathbf{M}_B}{|\mathbf{M}_A||\mathbf{M}_B|}, \tag{2}$$

where J_1 is the bilinear exchange constant.

The dynamic problem has been faced numerically solving the Landau-Lifshitz equations expressed, for each film *l*, as[25]

$$-\frac{1}{\gamma}\frac{\partial\mathbf{M}_l}{\partial t} = \mathbf{M}_l\times\mathbf{H}_l^{\mathrm{eff}}, \tag{3}$$

where $\gamma = \gamma_e g/2$ is the gyromagnetic ratio with $\gamma_e = 1.759\times10^7$ Hz/Oe the electronic gyromagnetic ratio, and g the splitting factor for Fe. $\mathbf{H}_l^{\mathrm{eff}}$ is the effective magnetic field of the lth layer given by

$$\mathbf{H}_l^{\mathrm{eff}} = \mathbf{H} - \frac{1}{M_{sl}}\nabla U_l^{\mathrm{an}} + \mathbf{H}_{\mathrm{exch}} + \frac{2A_l}{M_{sl}}\boldsymbol{\nabla}^2 M_l + \mathbf{H}_l^{\mathrm{d}}. \tag{4}$$

The second term on the right side is the out-of-plane anisotropy magnetic field, $\mathbf{H}_{\mathrm{exch}}$ is the interlayer exchange field including the bilinear coupling, the fourth term is the intralayer exchange field with A_l and M_{sl} the exchange stiffness constant and the saturation magnetization, respectively, of the lth film, and $\mathbf{H}_l^{\mathrm{d}}$ is the dipolar field of the lth film. By expanding the total magnetization for each film to first order in the dynamic magnetization, the dynamical equations may be expressed in a matrix form as[26]

$$\sum_{j=1}^{4}[\alpha_{ij} + \beta_{ij}]m_j = 0 \tag{5}$$

with $m_1(m_3)$ and $m_2(m_4)$ the x and y dynamic magnetization components of film $A(B)$, respectively. α_{ij} is a function of the second derivatives of the energy density with respect to the azimuthal and polar angles and β_{ij} is the q-dependent correction matrix to first and second perturbative order in the propagation vector. The former gives the magnon frequencies in the long-wavelength limit,[27] while the latter takes the dipolar and the intralayer exchange fields into account. In our system they assume the following expressions:

$$\alpha_{ij}=\begin{bmatrix} -\frac{E_{\phi_A\phi_A}}{d_A} & \frac{E_{\phi_A\theta_A}}{d_A}-i\frac{\omega}{\gamma}M_A & -\frac{E_{\phi_A\phi_B}}{d_B} & \frac{E_{\phi_A\theta_B}}{d_B} \\ -\frac{E_{\theta_A\phi_A}}{d_A}-i\frac{\omega}{\gamma}M_A & \frac{E_{\theta_A\theta_A}}{d_A} & -\frac{E_{\theta_A\phi_B}}{d_B} & \frac{E_{\theta_A\theta_B}}{d_B} \\ -\frac{E_{\phi_B\phi_A}}{d_A} & \frac{E_{\phi_B\theta_A}}{d_A} & -\frac{E_{\phi_B\phi_B}}{d_B} & \frac{E_{\phi_B\theta_B}}{d_B}-i\frac{\omega}{\gamma}M_B \\ -\frac{E_{\theta_B\phi_A}}{d_A} & \frac{E_{\theta_B\theta_A}}{d_A} & -\frac{E_{\theta_B\phi_B}}{d_B}-i\frac{\omega}{\gamma}M_B & \frac{E_{\theta_B\theta_B}}{d_B} \end{bmatrix}, \tag{6}$$

where the subscripts indicate the second derivates with respect to the angles ϕ and θ and

$$\beta_{ij}=2\pi\begin{bmatrix} -|\mathbf{q}|d_A M_A^2-\frac{A_A}{\pi}q^2 & 0 & -|\mathbf{q}|d_A M_A M_B & q\,d_A i M_A M_B \\ 0 & -|\mathbf{q}|d_A M_A^2+\frac{A_A}{\pi}q^2 & -q\,d_A i M_A M_B & -|\mathbf{q}|d_A M_A M_B \\ -|\mathbf{q}|d_B M_A M_B & -q\,d_B i M_A M_B & -|\mathbf{q}|d_B M_B^2-\frac{A_B}{\pi}q^2 & 0 \\ q\,d_B i M_A M_B & -|\mathbf{q}|d_B M_A M_B & 0 & -|\mathbf{q}|d_B M_B^2+\frac{A_B}{\pi}q^2 \end{bmatrix}. \tag{7}$$

The matrix elements linear in the magnon wave vector are of dipolar nature, while the terms quadratic in q originate from the intralayer exchange couplings. The magnon frequencies have been obtained imposing that the determinant of $\alpha+\beta$ vanishes at various external fields H. For a fixed $\mathbf{q}$ the negative solutions are Stokes frequencies, while the positive ones are anti-Stokes frequencies. As a consequence of the dipolar correction term, Stokes and anti-Stokes frequencies are not symmetric. The solutions of Eq. (5) give the complex x and y components of the dynamic magnetization for each layer. The multiplicative constant is determined imposing that the average excitation energy[8] of each normal mode is equal to K_BT with K_B Boltzmann constant and T temperature of the thermic bath in contact with the magnetic system. The evaluation of the scattered electric field $\mathbf{E}_s$ represents the main step in the calculation of the scattering cross section. $\mathbf{E}_s$ is proportional to the magnetization-dependent dielectric tensor fluctuation $\delta\epsilon$.[28] In the calculation of $\delta\epsilon$ we have considered the first-order magneto-optic effect. This means that the tensor is proportional to the complex K Faraday constant and is linear in the dynamic magnetization components. Therefore only the off-diagonal tensor terms contribute to light-scattering from spin-waves since the diagonal ones are zero. We have applied the Green's-functions formalism to solve the propagation equation to first order in the scattered field $\mathbf{E}_s$. The Brillouin scattering differential cross section

$$\frac{d^2\sigma}{d\Omega\, d\omega}=C\,N(\omega)\frac{|\mathbf{E}_s|^2}{|\mathbf{E}_0|^2} \tag{8}$$

is proportional to the square of the scattered field $\mathbf{E}_s$ and depends on the usual thermic Bose-Einstein $N(\omega)$ factor, which, at room temperature is approximated by $K_BT/\hbar\omega$. The constant C is expressed in terms of optical and geometrical properties of the system.[19,29]

V. RESULTS AND DISCUSSION

For thicknesses of the Cu spacer larger than 6 Å, the measured Brillouin spectra consist of two spin-wave modes due to the Fe double layered structure. The absence of such two-peaks structure in the low Cu coverage range ($d_{Cu}=3$ and 6 Å) can be associated to a direct contact between the two magnetic layers through pinholes caused by interface roughness. Both the measured BLS frequencies and the calculated fitting curves (two branches) are shown in Fig. 3 for some Cu spacer thickness. For the whole range of thicknesses analyzed one observes that the frequency of both modes increases almost linearly with H. Magnetic parameters have been extracted by fitting the calculated spin-wave frequency to the experimental behavior.

In the fit procedure we have kept fixed the intralayer exchange stiffness constant of both layers at its value for bcc iron ($2.0\,\mu$ erg/cm) and we have fixed the interface anisotropy constants to the value obtained for the single iron film[11]: $K_A^s=K_B^s=0.43\pm0.02$ erg/cm^2 . We have used the splitting factor $g=2.09$, a typical fitted value for iron,[4] and the saturation magnetization of each film has been adjusted around its Fe bulk value, i.e., $4\pi M_S=21$ kOe. For the entire range of Cu spacer analyzed, we have obtained from a best fit procedure the following values for the first-order anisotropy constants of each film: $K_A^V=(3.45\pm0.2)\times10^6$ erg/cm^3, $K_B^V=(1.75\pm0.2)\times10^6$ erg/cm^3. The positive sign of the interface anisotropy indicates that the surface normal is a magnetic easy axis, even if, owing to the dominant shape anisotropy, the magnetization lies in the film plane. We have found two different values for the volume anisot-

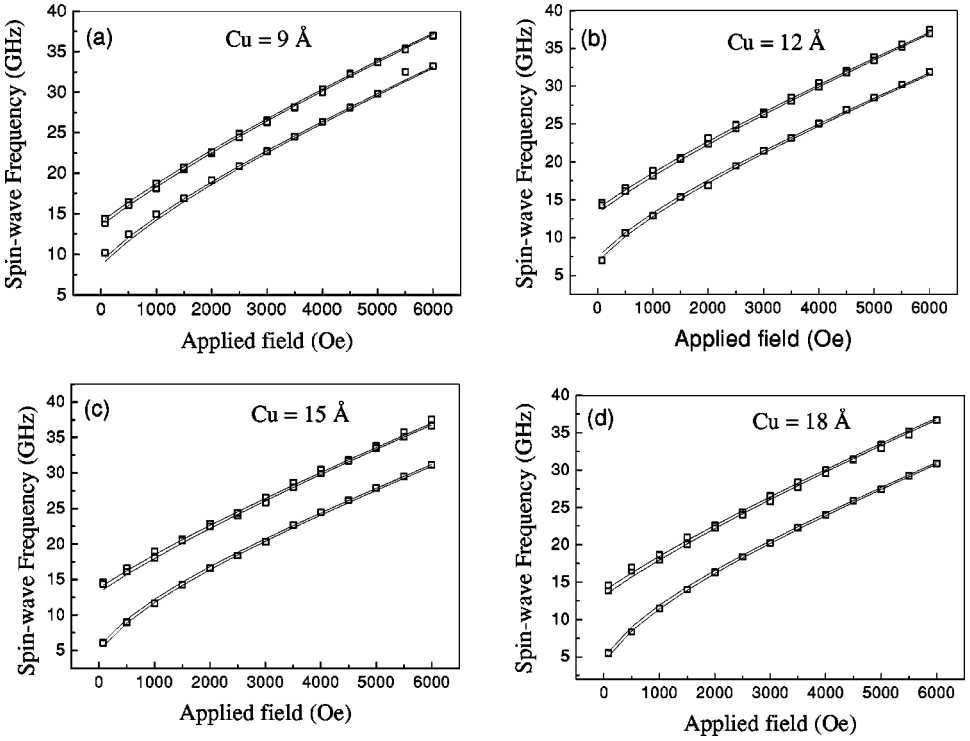

FIG. 3. Magnon frequencies vs H for various Cu interlayer thicknesses. Open squares: BLS data. Lines: calculated frequencies.

ropy constant in the two layers. This behavior is due to the geometrical asymmetry of the system which lowers the volume anisotropy of the thicker layer. The average of K_A^V and K_B^V gives a numerical value very close to the one fitted very recently for the single film.[11] In addition, the values of K_A^V and K_B^V are rather larger than the magnetocrystalline volume anisotropy for bulk Fe,[30] indicating that some additional contributions such as, for example, magnetoelastic anisotropy, comes to play a significant role in determining the magnetic anisotropy.

The obtained values of J_1, as depicted in Fig. 4, are always positive indicating a ferromagnetic coupling, in agreement with the shape of the Kerr hysteresis loops.[31] A comparison with the Mössbauer results on Fe(110)/Cu(111) multilayers of Freeland *et al.*[6] shows a qualitatively similar behavior even if their data accounted for a much more evident oscillatory component superimposed to the monotonic decrease. The effect of J_1 is more pronounced on the fit of the low-frequency mode as a function of the external field H, which is the most sensitive to the exchange between the two films. To reproduce the slope of the low-frequency mode, especially at low fields H, the bilinear term assumes a considerable importance. The absence of any antiferromagnetic coupling can be due to the high curvature of the Fermi surface near the extremal spanning vectors for the (111) orientation, if compared, for instance, to the (100) orientation.[32] In these conditions, even the presence of a slight bias field resulting from growth artifact can be sufficient to mask any antiferromagnetic coupling.

In Fig. 5, the BLS frequency data and the fitting curves are drawn, for a fixed applied field $H=1$ kOe, as a function of Cu spacer thickness. The agreement between theoretical calculations and BLS data is very good for both the high- and the low-frequency branch. The fit curves reproduce the gap between the two branches, which remains approximately constant for Cu thickness above 18 Å with only little variations strictly related to the oscillations of exchange coupling.

Figure 6 shows the comparison between the cross-section calculations and the BLS spectra for three different Cu spacers at low and high external field H and in the limit of single

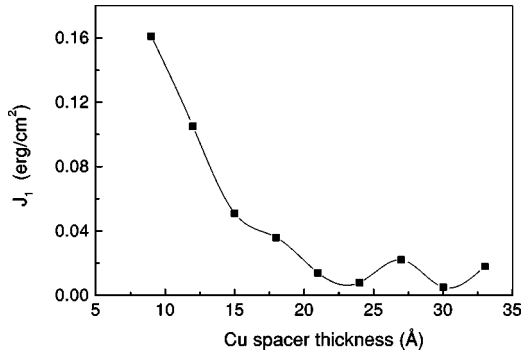

FIG. 4. J_1 vs Cu spacer. Full circles: fitted values. Line: guide to the eye.

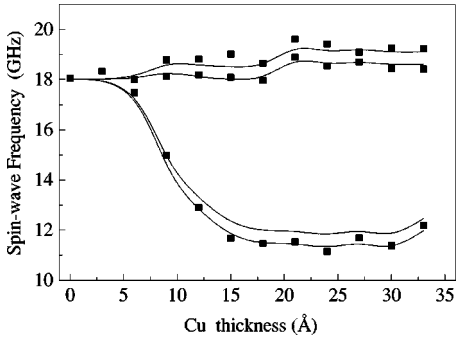

FIG. 5. Magnon frequencies as a function of Cu thickness at $H=1$ kOe. Symbols are experimental points. Line: calculated values.

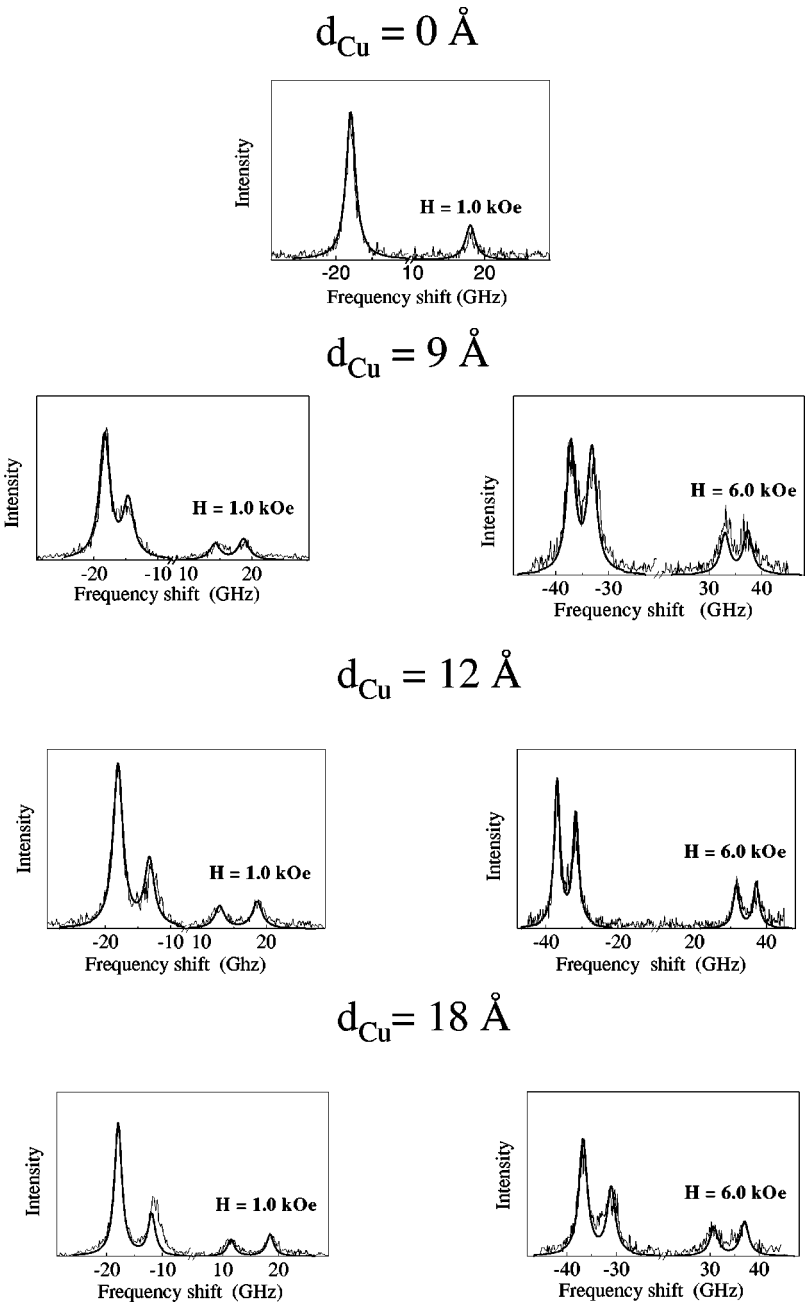

FIG. 6. BLS experimental spectra compared to calculated scattering cross sections for various Cu spacer thicknesses and at different magnetic fields. For $d_{Cu}=0$ the comparison is shown only at low field. Thin lines: experimental spectra. Bold lines: calculated spectra.

film ($d_{Cu}=0$) at low magnetic fields. The agreement between the experimental data and the theoretical results is good for all the Cu spacers investigated. A common feature of the BLS spectra is the asymmetry of the intensity peaks on the Stokes side, which becomes less evident at high applied fields. The highest intensity peak corresponds to the Damon-Eshbach mode, whereas the lowest intensity peak is related to the exchange mode, the most sensitive in frequency to J_1. The Damon-Eshbach mode is present in the thicker layer B, which gives the greatest contribution to the BLS peak. The nature of this mode is acoustical since both components of the dynamic magnetization precess in-phase. Due to its nonreciprocal nature, it becomes much less pronounced on the anti-Stokes side. The exchange mode is at a lower frequency and it is not preferentially present on film *A* or *B*. It is an optical mode given by the out-of-phase precession of the dynamic magnetizations of the two films. The Stokes anti-Stokes asymmetry of the exchange mode is related to the sign of the two dynamic magnetization components. For the Stokes exchange mode the respective components of the dynamic magnetization are of the same sign in each layer, whereas for that on the anti-Stokes side they are of opposite sign in the whole range of external fields applied. The effect on the cross section is represented by a greater cancellation for the peak on the anti-Stokes side with respect to the correspondent on the Stokes side.

In Fig. 6 one notes that the intensity of the exchange mode increases with increasing external field *H* and becomes almost comparable to that of the Damon-Eshbach mode at high fields. The contribution of the inner layer *B* to the scattering cross-section of this mode is small when *H* is high, so the interference between the out-of-phase dynamic magnetizations of the two layers is slight. Due to the out-of-plane anisotropy energy modelling the system, the greatest contri-

bution to the scattering cross section for both modes is given by the y component of the dynamic magnetization in the entire range of applied fields.

VI. CONCLUSIONS

In summary, we have grown a sequence of high quality thin metallic films on the 7×7 reconstructed surface of Si(111) substrate using a Cu buffer layer. From the frequencies of the spin-wave modes, a positive value of the bilinear interlayer exchange coupling J_1 was measured indicating a ferromagnetic exchange coupling of the two iron films. The BLS cross section was calculated using a simple model wich assumes the magnetization profile uniform within the films. The comparison between experimental spectra and scattering cross-section calculations is very satisfactory especially at high applied fields.

ACKNOWLEDGMENTS

This work has been developed in the framework of the INFM Project SIMBRIS. The authors would like to thank R. Bernardini for sample preparation.

[1] P. Swiatek, F. Saurenbach, Y. Pang, P. Grünberg, and W. Zinn, J. Appl. Phys. **61**, 3753 (1987).
[2] M. Vohl, J. Barnaś, and P. Grünberg, Phys. Rev. B **39**, 12 003 (1989).
[3] M. Vohl, J.A. Wolf, P. Grünberg, K. Spörl, D. Weller, and B. Zeper, J. Magn. Magn. Mater. **93**, 403 (1991).
[4] J.F. Cochran, J. Rudd, W.B. Muir, B. Heinrich, and Z. Celinski, Phys. Rev. B **42**, 508 (1990).
[5] B. Heinrich, Z. Celinski, J.F. Cochran, A.S. Arrott, K. Myrtle, and S.T. Purcell, Phys. Rev. B **47**, 5077 (1993).
[6] J.W. Freeland, D.J. Keavney, D.F. Storm, I.L. Grigorov, J.C. Walker, M.G. Pini, P. Politi, and A. Rettori, Phys. Rev. B **54**, 9942 (1996).
[7] J.F. Cochran and J.R. Dutcher, J. Appl. Phys. **64**, 6092 (1988).
[8] J.F. Cochran and J.R. Dutcher, J. Magn. Magn. Mater. **73**, 299 (1988); J. Appl. Phys. **63**, 3814 (1988).
[9] Y. Roussigné, F. Ganot, C. Dugautier, P. Moch, and D. Renard, Phys. Rev. B **52**, 350 (1995).
[10] G. Gubbiotti, L. Albini, G. Carlotti, S. Loreti, C. Minarini, and M. De Crescenzi, Surf. Sci. **433-435**, 685 (1999).
[11] G. Gubbiotti, L. Albini, S. Tacchi, G. Carlotti, R. Gunnella, and M. De Crescenzi, Phys. Rev. B **60**, 17 150 (1999).
[12] G. A. Prinz, in *Ultrathin Magnetic Structures II*, edited by B. Heinrich and J. A. C. Bland (Springer-Verlag, Berlin, 1994), p. 1.
[13] A. Zangwill, *Physics at Surfaces* (Cambridge University Press, 1988), p. 422.
[14] R. Ramirez, A. Rahman, and I.K. Schuller, Phys. Rev. B **30**, 6208 (1984).
[15] D. Tian, F. Jona, and P.M. Marcus, Phys. Rev. B **45**, 11 216 (1992).
[16] J. Shen, M. Klaua, P. Ohresser, H. Jenniches, J. Barthel, Ch.V. Mohan, and J. Kirschner, Phys. Rev. B **56**, 11 134 (1997).
[17] G. Gubbiotti, G. Carlotti, F. D'Orazio, F. Lucari, R. Gunnella, and M. De Crescenzi, Surf. Sci. **454-456**, 891 (2000).
[18] J. R. Sandercock, in *Light Scattering in Solids III*, edited by Springer Series in Topics in Applied Physics Vol. 51 M. Cardona and G. Güntherodt (Springer-Verlag, Berlin, 1982), p. 173.
[19] G. Carlotti and G. Gubbiotti, La Rivista Italiana del Nuovo Cimento, Vol. 22, N.12, p. 10 (1999).
[20] G. Gubbiotti, G. Carlotti, G. Socino, F. D'Orazio, F. Lucari, R. Bernardini, and M. De Crescenzi, Phys. Rev. B **56**, 11 073 (1997).
[21] G. Gubbiotti, G. Carlotti, C. Minarini, S. Loreti, R. Gunnella, and M. De Crescenzi, Surf. Sci. **449**, 218–226 (2000).
[22] R.W. Wang and D.L. Mills, Phys. Rev. B **50**, 3931 (1994).
[23] M.J. Pechan and I.K. Schuller, Phys. Rev. Lett. **59**, 132 (1987).
[24] W. J. M. De Jonge, P. J. H. Bloemen, and F. J. A. Broeder, in *Ultrathin Magnetic Structures I*, edited by J. A. C. Bland and B. Heinrich (Springer-Verlag, Berlin, 1994), p. 65.
[25] B. Hillebrands, in *Light Scattering in Solids VII*, Springer Series on Applied Physics, edited by M. Cardona and G. Güntherodt (Springer-Verlag, Berlin, 2000), p. 8.
[26] M. Grimsditch, S. Kumar, and E.E. Fullerton, Phys. Rev. B **54**, 3385 (1996).
[27] J. Smit and H.G. Beljers, Philips Res. Rep. **10**, 113 (1955).
[28] R.E. Camley and D.L. Mills, Phys. Rev. B **18**, 4821 (1978).
[29] S.O. Demokritov and E. Tsymbal, J. Phys.: Condens. Matter **6**, 7145 (1994).
[30] E. P. Wohlfarth, in *Ferromagnetic Materials*, edited by E. P. Wohlfarth (North-Holland, Amsterdam, 1980), p. 39.
[31] G. Gubbiotti, L. Albini, G. Carlotti, A. Montecchiari, M. De Crescenzi, R. Zivieri, L. Giovannini, and F. Nizzoli (unpublished).
[32] P. Bruno and C. Chappert, Phys. Rev. B **46**, 261 (1992).